Materials Science and Engineering A 512 (2009) 67–75

Contents lists available at ScienceDirect

Materials Science and Engineering A

journal homepage: www.elsevier.com/locate/msea

Temperature and direction dependence of internal strain and texture evolution during deformation of uranium

D.W. Brown*, M.A.M. Bourke, B. Clausen, D.R. Korzekwa, R.C. Korzekwa, R.J. McCabe, T.A. Sisneros, D.F. Teter

Los Alamos National Laboratory, Los Alamos, NM 87545, USA

ARTICLE INFO

Article history:
Received 23 July 2008
Received in revised form 5 January 2009
Accepted 4 February 2009

Keywords:
Uranium
Deformation
Neutron diffraction
Internal stresses
Texture

ABSTRACT

Depleted uranium is of current programmatic interest at Los Alamos National Lab due to its high density and nuclear applications. At room temperature, depleted uranium displays an orthorhombic crystal structure with highly anisotropic mechanical and thermal properties. For instance, the coefficient of thermal expansion is roughly $20 \times 10^{-6}\,^{\circ}C^{-1}$ in the *a* and *c* directions, but near zero or slightly negative in the *b* direction. The innate anisotropy combined with thermo-mechanical processing during manufacture results in spatially varying residual stresses and crystallographic texture, which can cause distortion, and failure in completed parts, effectively wasting resources. This paper focuses on the development of residual stresses and textures during deformation at room and elevated temperatures with an eye on the future development of computational polycrystalline plasticity models based on the known micro-mechanical deformation mechanisms of the material.

1. Introduction

Neutron diffraction and, more recently, high-energy synchrotron X-ray diffraction are generally accepted techniques used for the measurement of bulk residual stresses in thermo-mechanically processed (rolled, welded, etc.) parts. These techniques rely on the spatially resolved measurement of variations of lattice parameters or interplanar spacings (lattice strains) of given grain orientations and subsequent conversion of the measured strains to stresses. It is well known that intergranular or type II strains add confusion to the measurement of residual stresses with diffraction techniques and various schemes for minimizing these have been proposed and will be discussed in the following.

The earliest such method was to utilize the strains measured in a single grain orientation (*h k l*) that is minimally effected by intergranular strains, for instance, the (3 1 1) peak in fcc steel [1]. More recently, the use of time-of-flight (TOF) neutron diffraction at spallation neutron sources, which yields a large section of the diffraction pattern with a single diffraction vector, allows determination of lattice parameters with Rietveld analysis of the diffraction pattern. The lattice parameter so determined represents an empirical average over all crystal orientations present [2]. Daymond et al. [3] demonstrated that strains in cubic steel determined from Rietveld refinement of the lattice parameter represented the bulk response at least as accurately as single peak analysis.

Determination of representative residual stresses from hexagonal and lower symmetry materials is considerably more difficult because of increased anisotropy (intergranular strains) and multiple lattice parameters that define the crystal structure. Daymond et al. [4] showed that an appropriate texture weighted average of the **a** and **c** strains measured in beryllium was representative of the bulk response. Recently, Daymond developed a more physically based weighting scheme for the determination of representative residual stresses from both single peak and lattice parameter strain measurements [5] and demonstrated its value in cubic steel and hexagonal titanium.

Orthorhombic α-uranium represents the next step in complexity. Also, residual stresses in formed and welded uranium parts are of considerable interest to defense and energy generation applications. Cahn [6,7] first enumerated the active deformation modes, both slip and twinning, in single crystalline α-uranium. Calnan and Clews used these deformation modes, with no experimental determination of the relative critical resolved shear stresses (crss's) to qualitatively predict the deformation texture of uranium under tension, compression and rolling, but at the time had no measured textures with which to compare. Morris [8] reported the first measurement of the rolling texture of α-uranium with X-ray diffraction in 1971. In 1991, Rollett measured and modeled texture development in polycrystalline α-uranium under multiple deformation geometries

* Corresponding author. Tel.: +1 505 667 7904; fax: +1 505 665 2676.
E-mail address: dbrown@lanl.gov (D.W. Brown).

0921-5093/$ – see front matter © 2009 Published by Elsevier B.V.
doi:10.1016/j.msea.2009.02.004

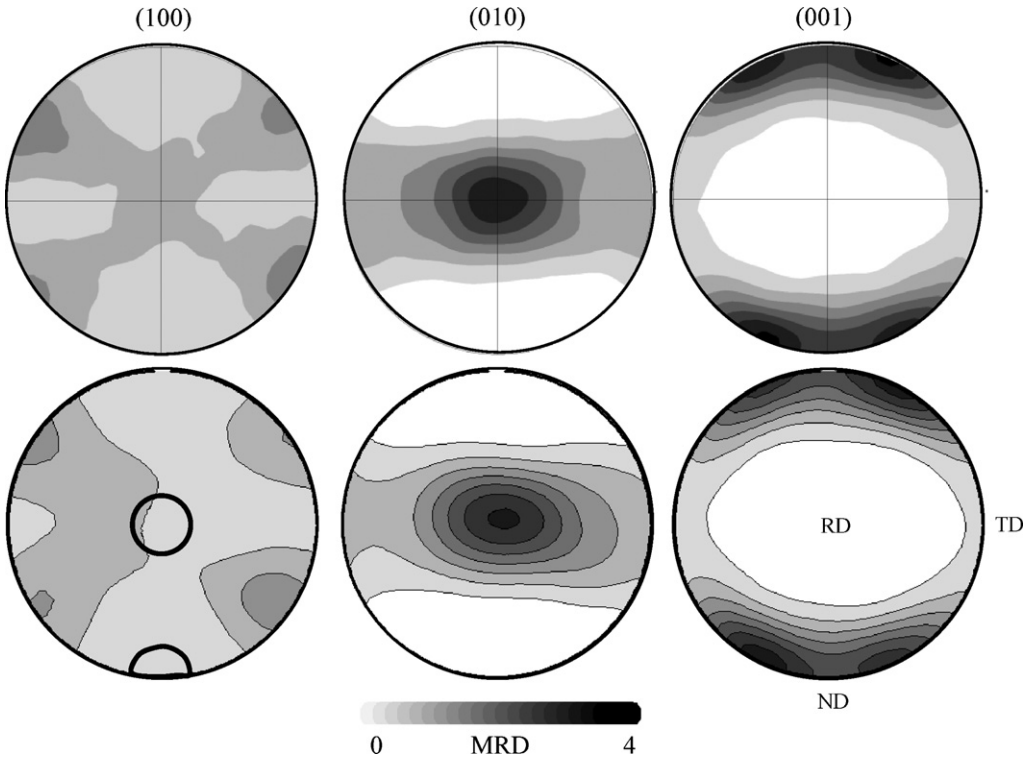

Fig. 1. (1 0 0), (0 1 0) and (0 0 1) pole figures measured on the as-rolled uranium plates. The final rolling direction (RD), transverse direction (TD), and plate normal direction (ND) are indicated. The contours go linearly from 0 to 4 at 0.5 multiples of random distribution (MRD) intervals. The circle in the center of the (1 0 0) pole roughly represents the detector acceptance of the SMARTS detector with diffraction vector parallel to the load axis.

using crss's found by Daniel et al. [9] on single crystal uranium.

This paper represents a focused study on the crystallographic response of uranium to applied stress as a function of temperature with an eye toward interpretation of spatially resolved lattice parameter measurements in specific formed uranium parts. In the long term, the goal is to couple grain-scale self-consistent models with macroscopic finite element analysis [10,11] to understand and predict the development of texture and residual stresses in complex formed parts through all steps of processing. In particular, it was motivated by a need to evaluate residual stresses in a deep drawn uranium part formed from a rolled plate. The stress applied during deep drawing of a plate is comprised mostly of in-plane biaxial tension. Due to the difficulty of performing biaxial tension or bulge tests *in situ*, we chose to study the microstructural response (internal strain and texture evolution) during uniaxial tension along both the rolling and transverse in-plane directions.

In situ neutron diffraction measurements during uniaxial tensile deformation of α-uranium at room temperature, 200 °C, and 400 °C were completed. Both single peak and lattice parameters strains were determined and are presented. Complete orientation distribution functions were determined *ex situ* in the as-rolled state as well as after 5% and 20% plastic strain.

2. Experimental techniques

2.1. Sample preparation

The depleted uranium was initially cast into a 254 mm thick ingot. The ingot was first hot cross-rolled at 640 °C to 32 mm then warm clock-rolled at 330 °C to 15 mm before an intermediate anneal of 480 °C for 2 h. Subsequently, the plate was further warm clock-rolled at 330 °C to 7.6 mm and given a final anneal of 550 °C for 2 h. Pin-grip dog-bone tensile specimens were electro-discharge machined from the rolled plate with tensile axes parallel (RD) and transverse (TD) to the final rolling direction.

The as-rolled texture of the plate determined by neutron diffraction and EBSD is shown in Fig. 1. The two techniques are in excellent agreement. The crystallographic texture is defined by the *b*-axes predominantly oriented along the final rolling direction (RD) with *c*-axes and *a*-axes slightly offset from the plate normal (ND) and transverse direction (TD), respectively. The microstructure of the rolled material is highlighted in Fig. 2a by the EBSD orientation map taken on a cross-section of the sample where the surface normal is parallel to the final rolling direction. The initial microstructure consists of equiaxed grains with a grain size of approximately 25 μm.

2.2. Neutron diffraction techniques

Neutron diffraction measurements of internal strain and bulk texture were performed on the Spectrometer for Materials Research at Temperature and Stress (SMARTS) and High Pressure Preferred Orientation (HIPPO) instruments, respectively, at the Manuel Lujan Jr. Neutron Scattering Center, LANSCE, Los Alamos National Laboratory. Details of the diffraction instruments are similar and published elsewhere [12,13] and only a short description is presented here.

SMARTS has a 30 m incident flight path yielding an instrumental resolution of $\Delta d/d = 2.5 \times 10^{-3}$ (FWHM), making it suitable to measure the small shifts in lattice spacing associated with internal strains. A purpose built horizontal load frame was utilized to perform *in situ* measurements of the lattice strains during uniaxial tension. Fig. 3 shows a schematic of SMARTS indicating the sample geometry and orientation of the applied stress relative to the instrument. The load axis was oriented at 45° relative to the incident beam. Detectors on either side of the specimen simultaneously record data with diffraction vectors, parallel $Q_{\parallel}$ (−90°) and transverse $Q_{\perp}$ (+90°), to the applied load. Both detector banks have acceptance angles of ±15° in the vertical and horizontal directions.

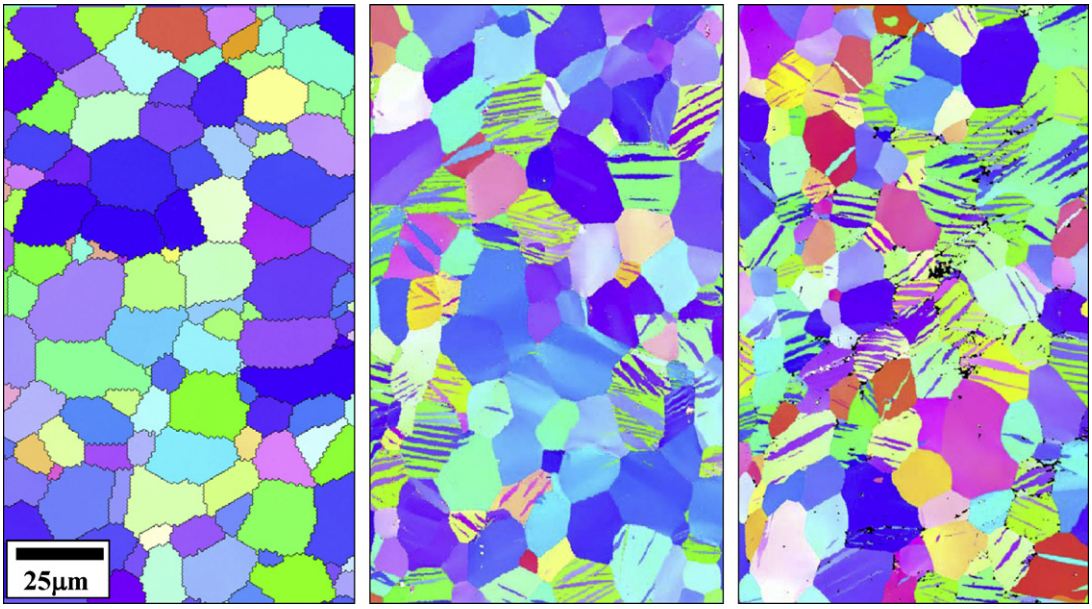

Fig. 2. EBSD orientation maps collected on the (a) as-rolled plate, and after 5% deformation in the (b) RD and (c) TD directions. Images show the specimen normal directions which are (a) RD, (b) RD, and (c) TD directions.

The circles drawn on the (0 0 1) pole figure in Fig. 1 schematically represent the acceptance area of the SMARTS detectors on the pole figure. The macroscopic strain achieved in the sample was measured concurrently using an extensometer that spanned the irradiated region.

In contrast, the HIPPO diffractometer has a 9 m flight path, which maximizes the incident neutron intensity for measurements of bulk texture. A robotic sample position system picks each sample from a tray and places it at beam center. With the 29 independent detector banks on HIPPO only four sample rotations are necessary to obtain sufficient coverage of sample space to produce complete orientation distribution functions. Rietveld analysis of 98 selected diffraction patterns using eighth order spherical harmonics with no assumed sample symmetry to describe the texture [14] was completed with the General Structure Analysis System (GSAS) software developed at LANSCE [15]. The observed orientation distributions

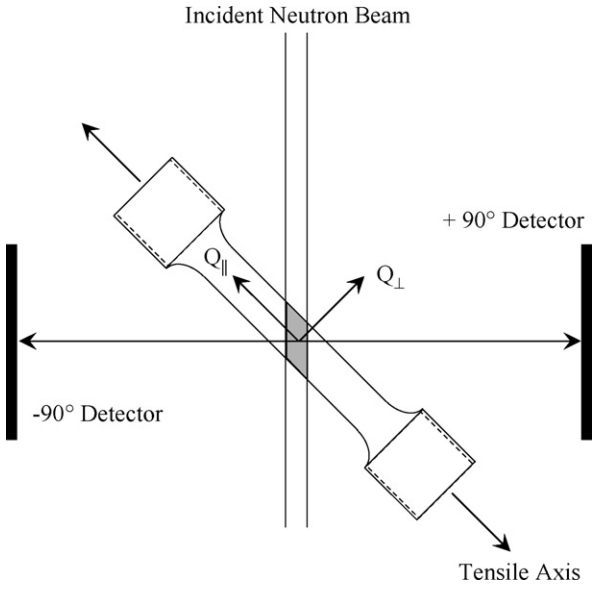

Fig. 3. Schematic of the diffraction geometry showing the scattering vectors $Q_{\parallel}$ and $Q_{\perp}$ relative to tensile axis of sample. Note, the drawing is not to scale.

are moderate, and relatively smooth. The use of higher order spherical harmonics does not significantly improve the fit, as indicated by the residual, but can add oscillations to the orientation distribution which are unphysical.

2.3. Interpretation of neutron diffraction measurements

Prior to showing the results of the neutron diffraction measurements, it is worthwhile to discuss precisely what is measured by diffraction and define common terminology used throughout the literature. Each diffraction peak ($h\,k\,l$) is comprised of neutrons diffracted from a unique subset of grains (grain family [5]) from within the irradiated volume with a common orientation, that is, a specific crystallographic plane normal ($h\,k\,l$) parallel to the diffraction vector. Three peak parameters, the position, intensity and breadth are commonly obtained from peak fits and each can be related to the microstructure. It is straightforward to relate the peak intensities to the crystallographic texture. The peak breadth is associated with small length scale heterogeneities within the grains such as defects and dislocations, although it is difficult to quantify this association, especially for lower symmetry materials. The peak position or, more precisely the change thereof, is related to the internal (lattice) strains of the grains. The interpretation of the variation of the lattice strains with applied stress can be unintuitive and we will discuss it in detail here.

It is important to remember that neutron diffraction directly measures elastic lattice strains, that is, changes in atomic spacings or lattice parameters. In a single grain, the elastic strain is necessarily proportional to the stress on that grain. From symmetry arguments, one can then assume that the elastic strain measured by diffraction on a family of grains with common orientation relative to the load axis is proportional to the average stress on that family of grains. That the elastic lattice strains in the "lattice strain vs. applied stress" plots that follow are not proportional to the applied stress is indicative of the difference between the macroscopic stress applied to the sample and the stress perceived by individual grain families. The deviation of the grain stress from the applied stress is attributable to grain-scale heterogeneities, in this case associated with elastic and plastic anisotropy of the material, resulting in local (grain scale) fluctuations away from the macroscopic stress field.

In a very real way, a plastically anisotropic polycrystalline sample may be considered as a complicated composite, in which each constituent grain family (orientation) has a different set of mechanical properties.

These orientation dependent grain-scale stress fluctuations are typically called intergranular stresses [5,16] or grain interaction stresses [17]. Similarly, the intergranular strains, $\varepsilon_{\text{int}}(h\,k\,l)$, are the difference between the elastic strain measured in a particular grain orientation $\varepsilon_{\text{int}}(h\,k\,l)$ and that expected based on the macroscopic applied stress (σ_{app}) and a suitable orientation dependent modulus (E_{hkl}):

$$\varepsilon_{\text{int}}(hkl) = \varepsilon(hkl) - \frac{\sigma_{\text{app}}}{E_{hkl}}. \quad (1)$$

Because we use the initial diffraction pattern at near zero load as a reference, the intergranular strains we will present are associated with plastic anisotropy, i.e. the strong dependence of the single crystal yield surface on the crystallographic orientation. That is to say, we ignore the intergranular strains related to the anisotropic coefficient of thermal expansion.

When plasticity initiates in a grain family with a given orientation with respect to the load axis, the rate of increase of the elastic lattice strain in that family decreases markedly. Elastic straining is replaced by plastic flow, to which the elastic lattice strains are insensitive. In the case of perfect plasticity, i.e. no hardening, the lattice strain saturates, and the lattice specific stress/strain curve becomes vertical. This grain family is typically referred to as plastically soft which should not be confused with elastically compliant.

Once (perfect) plasticity is initiated in a grain family, no further increments of stress will be supported by said grain family and other grain families respond by bearing a larger incremental load, and thus, increased incremental lattice strains, resulting in an apparent reduced modulus. These remaining elastic grains are typically referred to as plastically hard. The saturation of the elastic strains in plastically soft grains and apparent reduced modulus of plastically hard grains after plastic deformation initiates results in the characteristic "y" shape of "lattice strain vs. stress" plots commonly seen in the literature.

While plastic strain does not directly change the diffracted peak position (the elastic strain), it is manifested by increases in peak width. Profile function 1 in GSAS was used to fit the diffraction data in this study. The interpretation of the profile parameters is discussed in detail in the GSAS manual, and only a short description relevant to the peak broadening is given here. Profile 1 assumes a peak profile that is a convolution of two back-to-back exponentials with a Gaussian line shape defined by

$$G(\Delta T - \tau) = \frac{1}{\sqrt{2\pi\sigma^2}} \exp\left[\frac{-(\Delta T - \tau)^2}{2\sigma^2}\right],$$

where ΔT is the difference in time-of-flight between the reflection position and the profile point. The variance of the Gaussian profile is given by σ which is a function of d-space:

$$\sigma^2 = \sigma_0^2 + \sigma_1^2 d^2 + \sigma_2^2 d^4,$$

where, for simplicity, anisotropic peak broadening has been ignored. It is important to note that σ is fit over the entire profile, and is not specific to any ($h\,k\,l$). To generalize, strain broadening and instrumental resolution contribute to σ_1, and crystallite size broadening to σ_2. With the relatively poor peak width resolution of SMARTS, crystallite size broadening would only be observable with very small (sub-micron) size grains. Also, the crystallite size is not expected to change during the tensile tests to 20% deformation, and thus σ_2 was held fixed at zero. The amount of strain broadening

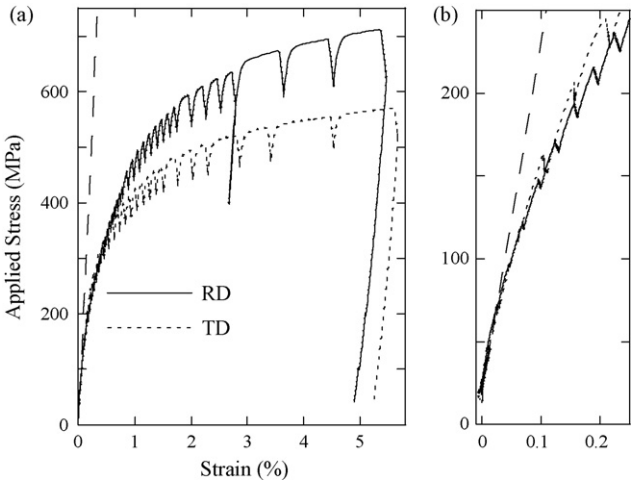

Fig. 4. (a) Uranium flow curves measured along the plate RD (solid line) and TD (dotted line). (b) An enlargement of the elastic region. The dashed lines represent a modulus of 190 GPa.

($\Delta d/d$) can be determined from the variance (σ_1) in percent by

$$S(\%) = \frac{1}{C}\sqrt{8\ln 2(\sigma_1^2 - \sigma_{1\text{i}}^2)} \times 100,$$

where $\sigma_{1\text{i}}$ represents the instrumental resolution and C is a diffractometer constant. The strain broadening term, S, is often referred to as "microstrain" or "intragranular strain", depending on the audience, and is due to a local distribution of interatomic spacings associated with defects, such as dislocations, or other heterogeneities such as twin boundaries or chemical variations.

We assume the peak variance of the initial diffraction pattern before deformation represents the instrumental resolution. The SMARTS diffractometer, in particular, has not been properly characterized for accurate determination of sample broadening and the peak resolution is poor relative to that of high-resolution synchrotron X-ray techniques. The instrumental resolution is of similar magnitude as the sample broadening observed with deformation. Thus, only qualitative information (trends) will be extracted from the data collected in this work.

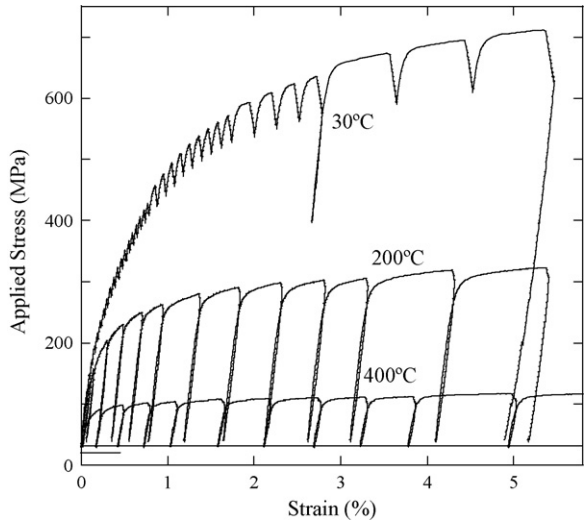

Fig. 5. Uranium flow curves measured along the plate RD at 30 °C, 200 °C, and 400 °C.

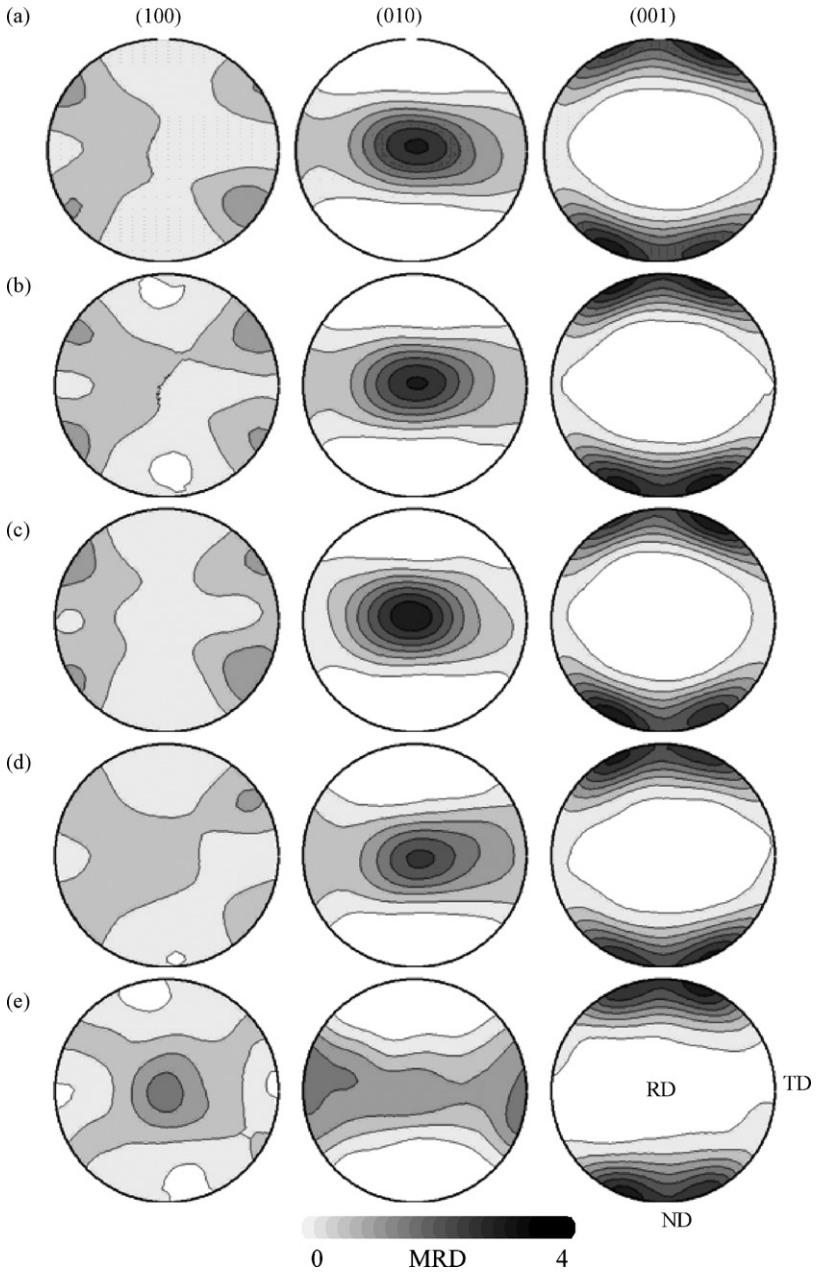

Fig. 6. (1 0 0), (0 1 0) and (0 0 1) pole figures measured (a) as-received and after (b) 5% and (c) 20% deformation along the RD and (d) 5% and (e) 20% deformation along the TD. The contours go from 0 to 4 at 0.5 MRD intervals.

3. Results

3.1. Macroscopic response

Fig. 4a shows the stress–strain curves measured during room temperature (30 °C) tensile deformation along the final rolling and transverse directions. Fig. 4b shows an enlargement of the elastic regime. The decreases in load occurred while the samples were held in position control while diffraction data was collected. It is difficult to see due to the scale of Fig. 4, but the observed flow curves exhibit a small amount of curvature even at small stresses during loading as well as during unloading making accurate determination of the macroscopic elastic modulus impossible and the yield point difficult. The elastic moduli in the RD, TD and ND directions calculated using the reported single crystal stiffness matrix [18] and an Eshelby type elastic self-consistent calculation [19] including the measured crystallographic texture shown in Fig. 1 are 187 GPa, 196 GPa, and 207 GPa, respectively. The dashed lines in Figs. 4a–b represent a modulus of 190 GPa and correspond well to the observed loading below 90 MPa. Both samples deviate from the linear elastic response at roughly 90 MPa and the 0.2% offset occurs at nearly 300 MPa. At small strains, i.e. less than 0.2%, the material appears to harden more rapidly when strained along the transverse direction, but the stress relaxation observed during the neutron collection makes this difficult to evaluate with confidence. Diffraction data was collected at more points during the RD deformation than the TD. Clearly, beyond roughly 0.5% strain, the hardening rate and thus flow stress is higher along the rolling direction, that is parallel to the dominant *b*-axis orientation.

Fig. 5 shows the flow curves measured during tensile deformation at 30 °C, 200 °C and 400 °C along the final rolling direction. The samples relaxed excessively when held at load at elevated

temperature while collecting diffraction data, so the samples were repeatedly loaded to incrementally increasing strains and immediately unloaded to a nominal stress of 40 MPa for collection of diffraction data. In this way, the orientation dependent intergranular or Type II residual strains were measured as a function of plastic strain. This technique has been demonstrated to provide substantively equivalent measurement of the intergranular strains when compared to monotonic loading in a zirconium alloy [20]. The flow stress decreased considerably with increased temperature. For instance, the flow stress at 1% deformation decreased from 480 MPa to 100 MPa when the deformation temperature increased from 30 °C to 400 °C. Also, the hardening rate is much lower at 400 °C.

3.2. Microstructural development

Fig. 2b and c shows the evolution of the microstructure after 5% deformation in the RD and TD, respectively. The orientation of the images is the same as Fig. 2a. A significant population of deformation twins is present for both deformation paths. The twins are predominantly of the {1 3 0} type, but a small amount of both {1 7 2} and {1 1 2} twins are also apparent. After 5% tensile deformation in the RD and TD directions, the volume fractions of {130} twins are 8% and 10%, respectively.

3.3. Texture development

Figs. 6a–e shows pole figures representing the crystallographic texture in the as-rolled state (a) and after 5% and 20% deformation in the rolling (b and c) and transverse directions (d and e), respectively. The neutron diffraction data from which the pole figures were determined was collected *ex situ* on the HIPPO diffractometer. Again, the EBSD and neutron diffraction textures were in agreement. Note that the pole figures are oriented such that the original coordinate system of the plate (Fig. 1) is maintained, i.e. the rolling normal direction is up the page and the final rolling direction is out of the page. Thus, in Fig. 6b and c the straining direction is out of the page; in Fig. 6d and e the straining direction is across the page. The initial texture and development are consistent with those previously found under similar loading conditions [21].

When loading parallel to the final rolling direction, the texture does not change after 5% plastic deformation to within our limits of observation. However, after 20% tensile deformation in the rolling direction, the (0 1 0) fiber parallel to the loading (rolling) direction does increase slightly, from a maximum pole density of 3.6 multiples of random distribution (MRD) prior to deformation to 3.9 MRD after. In contrast, the texture evolves much more notably during deformation transverse to the final rolling direction. Indeed, after only 5% tensile deformation transverse to the final rolling direction, the maximum (0 1 0) pole density has reduced from 3.6 MRD to 3.1 MRD and after 20% deformation along the transverse direction the predominant (0 1 0) orientation is now along the transverse direction. Concomitantly, the (1 0 0) poles align transverse to the straining direction, i.e. parallel to the rolling direction, while the (0 0 1) poles tend to stay aligned near the rolling normal direction.

Fig. 7a and b shows the development of the (2 0 0), (0 2 0), and (0 0 2) integrated peak intensity parallel to the straining direction measured *in situ* on the SMARTS diffractometer during tensile deformation along the rolling and transverse directions, respectively. The peak intensities are initially normalized to one so that they may be easily shown on a single plot. In the rolling direction, the (2 0 0) and (0 0 2) peaks are initially relatively weak and near stronger peaks. They show a small decrease in integrated intensity, and beyond roughly 3% deformation, the fit quality of these peaks deteriorates markedly. In contrast, during deformation in the transverse direction, the (0 2 0) peak parallel to the straining direction increases in intensity markedly, while the (2 0 0) and (0 0 2) decrease slightly.

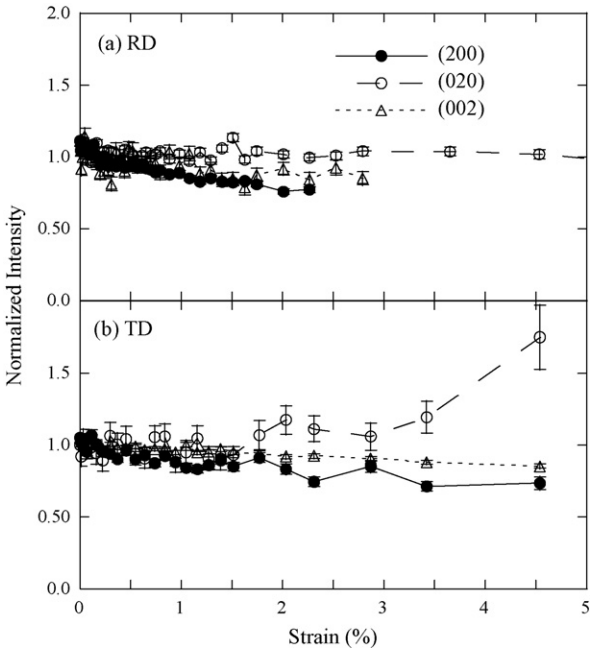

Fig. 7. Development of single peak intensity during tensile deformation (a) parallel to the final rolling direction (RD) and (b) the transverse direction (TD).

3.4. Increase of peak breadth with plastic strain

Fig. 8 shows the evolution of the strain broadening (sometimes called "microstrain" or "intragranular" strain) with increasing plastic strain during deformation at 30 °C in the transverse direction and at 30 °C, 200 °C and 400 °C in the rolling direction. Recall from the discussion above that the strain broadening parameter is determined from a full pattern fit, and is not specific to a given peak (*h k l*). The strain broadening measured in the samples deformed at 30 °C

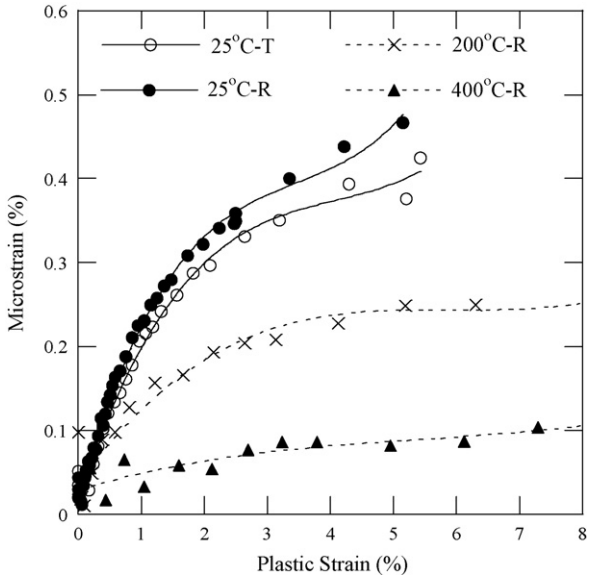

Fig. 8. Development of strain broadening as a function of plastic strain. The lines are guides to the eye.

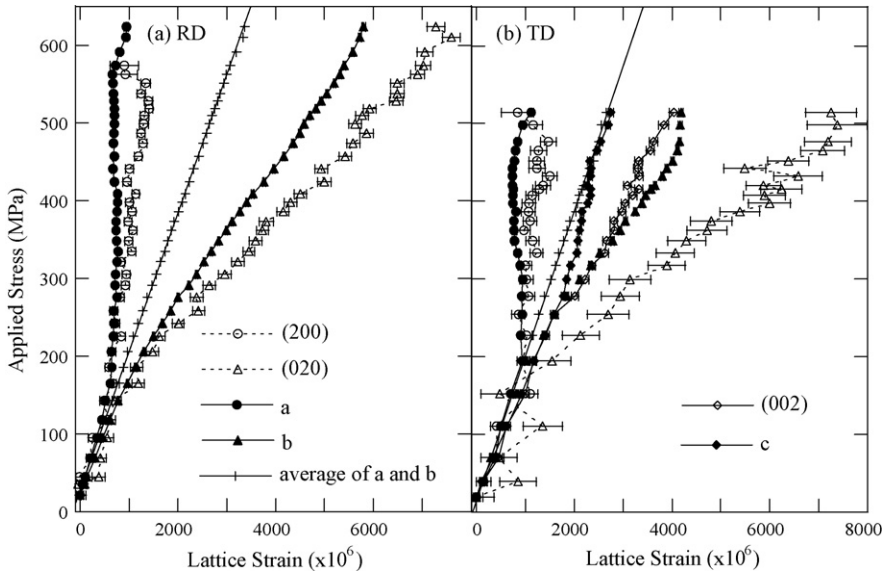

Fig. 9. Development of the elastic lattice strains in rolled uranium during tensile deformation in the (a) rolling (RD) and (b) transverse directions (TD). The filled and open symbols represent lattice parameter and single peak strains, respectively. The (+) signs represent the average of the **a** and **b** strain and the solid line a linear fit to that average.

along the rolling and transverse directions are very similar. In both cases, the variance increases monotonically with increased plastic strain. However, the evolution of the broadening with strain is clearly influenced by the increase in temperature. During deformation at 200 °C, the increase of the peak broadening is significantly reduced and at 400 °C the peak breadth remains nearly constant with deformation.

3.5. Development of lattice strains

The lattice parameter of the α-uranium (orthorhombic) measured with a nominal holding stress of 20 MPa were $a = 2.8515$ Å, $b = 5.8590$ Å, and $c = 4.5919$ Å with relative uncertainty (precision, not accuracy) of roughly 1×10^{-4} Å. We note that these are statistical uncertainties from the Rietveld refinement, and do not account for errors such as small positioning errors, which are not quantified, but can be larger, on the order 0.001 Å. This uncertainty represents our resolution of changes in lattice parameter (strains), not in absolute lattice parameter measurement.

Fig. 9a and b shows the development of the axial lattice strains (measured in the $Q_{||}$ detector bank) measured during tensile deformation of uranium in the rolling and transverse directions, respectively. Strains calculated for Rietveld refinements (lattice parameters) as well as single peak fits ($h\,k\,l$) are shown in the figures. Uncertainties in the lattice strains are indicated, but in some cases are smaller than the data points. The two measures of lattice strain yield similar results, and will be discussed concurrently. There are few *c*-axis directed along final rolling direction, and as such, relatively poor statistics are obtained for *c*-axis and (0 0 2) strains and they are omitted from Fig. 9a.

The development of the lattice strains is qualitatively similar during loading in the two sample directions despite the significant texture difference. Also, the single peak and corresponding lattice parameter strains behave qualitatively similar, for instance the (2 0 0) strains closely track the **a** strains. Recall that the (2 0 0) strains strictly represent the response of grains with their (2 0 0) pole parallel to the loading direction, while the **a** strains have contributions from all grain orientations ($h\,k\,l$) with a non-zero *h*. The **b**- and **c**-strains also qualitatively follow the (0 2 0) and (0 0 2) strains, respectively. As would be expected, the single orientation strains are always more extreme than those determined from the lattice parameter.

During tensile deformation in the final rolling direction, the lattice responds linearly with stress to roughly 150 MPa; roughly 200 MPa during straining in the transverse plate direction. Thus, the intergranular strains indicative of yielding are evident at stresses somewhat higher than the macroscopic deviation from linearity of 90 MPa (see Fig. 4b), but well below the 0.2 offset stress of 300 MPa. The slopes of the **a**, **b** and **c** strains in the elastic region of the transverse direction straining (where more data was collected in the elastic region) are 196 GPa, 169 GPa, and 141 GPa, respectively. In both rolling and transverse samples, beyond the elastic region the (2 0 0)/**a** strains saturate and no longer increase with subsequent incremental increases in applied stress. Concomitantly, the (0 2 0)/**b** strains respond by absorbing a greater portion of the elastic strain associated with subsequent stress increases. Due to the texture, the (0 0 2)/**c** strains were only measurable in the sample strained in the transverse plate direction and showed an intermediate behavior. The (0 0 2)/**c** strains initially accumulate more quickly after the saturation of the (2 0 0)/**a** strains, but themselves saturate above 300 MPa. Finally, an inflection is observed in the (020)/**b** strains, and corresponding inflection in the **a** and **c** strains, at roughly 450 MPa. It is interesting to note that the simple average of the **a** and **b** strains (the majority in-plane orientations) is linear with applied stress to the largest stresses achieved during deformation in both the rolling and transverse directions with slopes of 179 GPa and 187 GPa, respectively.

For purposes of clarity, data taken during unload are not shown. The elastic strains were not perfectly linear with unload, consistent with the non-linearity of the macroscopic unload curve. However, the deviation of the unload curves from linearity was insignificant compared to the non-linearity observed during loading.

4. Discussion

4.1. Room temperature deformation

We first attempt to relate the macroscopic data recorded by the load cell and extensometer to the microstructural information obtained from neutron diffraction. The dependence of both the macroscopic and microscopic results on the straining direction is small, given the relatively strong texture of the rolled uranium. Prior to the macroscopic yield point the lattice strains respond linearly to the applied stress and the peak widths remain constant. The

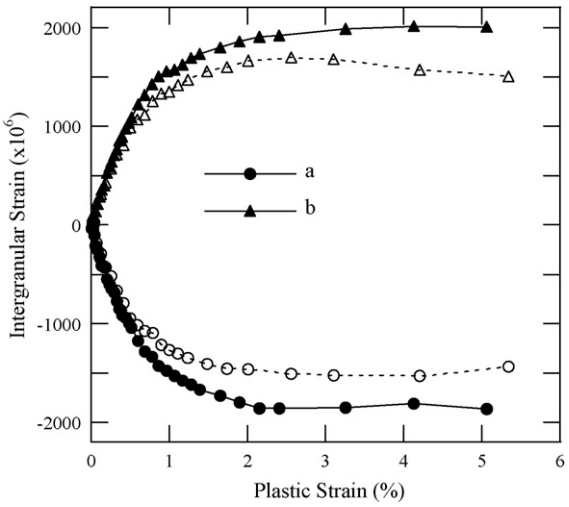

Fig. 10. Development of the intergranular strains during tensile deformation of rolled uranium along the rolling direction (open symbols) and transverse directions (filled symbols).

observed lattice strains first deviate from linear behavior near the macroscopic yield point of the samples and are a crystallographic indication of plasticity. As described above, the deviations of the lattice strains from linearity shown in Fig. 9 are associated with intergranular stresses that develop due to plastic anisotropy on the grain scale.

The intergranular strains that developed during room temperature deformation along the rolling and transverse directions, as determined from Eq. (1), are shown in Fig. 10. The development of the intergranular strains is similar during loading in the rolling and transverse directions. The intergranular strains increase (in an absolute sense) linearly until nearly 1% and saturate completely by 2.5% plastic strain. The intergranular strains during loading in the rolling direction are consistently lower than in the transverse direction. It is important to note that for reasonably small strains (<2%), the separation between the **a** and **b** intergranular strains may be parameterized as a function of the plastic strain and used to estimate the plastic strain history of thermo-mechanically processed parts [3,22].

It has been shown in several cases that the neutron diffraction texture measurements are quite sensitive to deformation twinning [23,24]. However, the deformation twins that are shown in the EBSD orientation map do not strongly affect the measured bulk texture at small strains as seen in reference [23,24]. At 5% strain, the twin volume fraction as determined by EBSD is low, roughly 10 volume percent, and the $\{1\,3\,0\}$ twin causes a roughly 69° rotation about the $\langle 0\,0\,1\rangle$ direction, which is a relatively symmetric direction in the orientation distribution. Moreover, due to the low symmetry of the material (i.e. the low number of equivalent slip systems), slip deformation will also act to quickly reorient the material. The small texture changes observed during the *in situ* measurements, decreases of $(2\,0\,0)$ intensity and increase of $(0\,1\,0)$ intensity parallel to the tensile straining, are consistent with $\{1\,3\,0\}$ twinning. However, future polycrystalline plasticity modeling work is necessary to deconvolute the texture evolution due to twinning and slip, as well as the evolution of the lattice strains.

Also, once plastic deformation initiates in the room temperature samples, the strain broadening rapidly increases. The strain broadening, or "microstrain", is related to lattice parameter variations on a very fine scale called intragranular strains. The increase in intragranular strain is difficult to interpret because it may be attributable to several different microstructure effects including dislocations, defects, twin boundaries, or heterogeneous stress distribution due to the plastic anisotropy. While it is attractive to attempt to calculate the plastic strain dependent dislocation density or twin boundary density, we feel the relatively large instrumental contribution to the peak profile as well as the complication arising from the anisotropic material would render the calculation inaccurate. Suffice it to note that the increase in intragranular strain is correlated with the increased flow stress of the material with plastic deformation (hardening).

4.2. Impact on macroscopic residual stress measurements

In spatially resolved measurements at time-of-flight neutron sources, which are always neutron flux limited, there is a substantial reduction of count time if lattice parameters, rather than single peak interplanar spacings, can be used to accurately characterize the macroscopic stress field. Since the lattice parameter and single peak strains behave at least qualitatively similarly, we will limit subsequent discussion to the lattice parameter strains.

At first glance, the situation represented in Fig. 9a and b would seem problematic for spatially resolved residual strain measurements because of the extraordinary plastic anisotropy of the material: residual strains measured with different orientations would yield dramatically different results. The averaging scheme of Daymond [5] was considered untenable in the specific thermo-mechanically processed parts that motivated this study, due to rapid spatial variations of the texture. However, it was found empirically that in both straining directions (rolling and transverse directions) the simple average of the **a** and **b** strains (**a** and **b** oriented grains are predominant in these directions) is linear with applied stress to the maximum stress/strain achieved in each sample. Moreover, the effective modulus of this average grain stain, 179 GPa and 187 GPa in the rolling and transverse directions, respectively, is relatively insensitive to sample orientation and reasonably close to the calculated macroscopic modulus in each direction of 187 MPa and 196 GPa, respectively. Overall, the average of the **a** and **b** strains makes an attractive empirical quantity for characterization of a spatially varying residual stress field in the uranium part of interest for this study, and likely for welded uranium plates as the texture and stress directions (predominantly in-plane) are likely similar.

4.3. Effect of deformation temperature on the development of the microstructure

As shown in Fig. 8, an increase in deformation temperature reduces the observed peak width increase with plastic strain. Again, the difficulty of deconvoluting the microstructural effects prevents interpretation of this result. As noted above however, the increase in intragranular strain is correlated with increased hardening of the material. As the deformation temperature is raised and the hardening is reduced, so too is the increase in intragranular strain. Thus, the defects or heterogeneities associated with the local (on the grain scale) distribution of interatomic spacing (that is the increased peak breadth) are annealed out to increasing degrees with increased deformation temperature.

Fig. 11 shows the development of the intergranular strains as a function of plastic strain at the three deformation temperatures. Recall (Fig. 5) that at elevated temperature the material relaxed too much to allow for holds at stress while neutrons were collected. Thus, the intergranular (or Type II residual) strains were measured directly by unloading to a nominal holding stress. The magnitude of the intergranular strains decreases strongly with increased deformation temperature and are not significantly different from zero at 400 °C. This indicates that the material has lost the ability to maintain stresses over short length scales (i.e. microstructural) at 400 °C. Coupled with the highly anisotropic coefficient of thermal expansion of uranium, the softening on the grain scale likely plays a

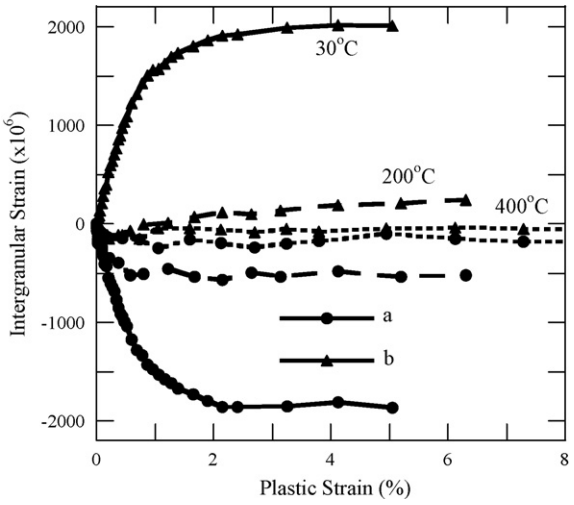

Fig. 11. Development of the intergranular strains during tensile deformation of rolled uranium along the rolling direction at 30 °C (solid lines), 200 °C (dashed lines) and 400 °C (dotted lines).

role in the reported thermal ratcheting (plastic deformation during thermal cycling) in uranium [25] (for example).

This is important information in particular when attempting to apply an elasto-plastic self-consistent (EPSC) model or Finite Element Analysis (FEA) to the deformation of depleted uranium. The EPSC model monitors the internal stresses in the grains including those developed during cooling from processing temperature due to the anisotropic CTE, which can be significant compared to the yield strength [16,26,27]. This result essentially sets the point at which the model must assume the material has enough rigidity to develop internal stresses. Obviously, the internal stresses developed during cooling increase in proportion to this temperature.

5. Conclusions

In situ neutron diffraction measurements of the development of internals stresses during in-plane (rolling and transverse directions) deformation of rolled uranium at room and elevated temperatures were completed. The texture was also measured with neutron diffraction in the as-rolled state as well as after 5% and 20% tensile deformation along final rolling and transverse directions of the plate. The texture consistently reoriented to align the *b*-axis, (0 2 0) plane normal, into alignment with the tensile straining direction. The texture evolution is likely due to combined effects of deformation twinning, seen explicitly using EBSD, and grain rotation caused by slip.

The development of internal strains was surprisingly insensitive to loading direction within the plane of the plate given the strong in-plane variation of the texture. Grains with their (2 0 0) plane normal (*a*-axis) parallel to the loading direction yielded first, at about 150 MPa and 200 MPa, during tensile straining in the rolling and transverse directions, respectively. The grain family with their (0 2 0) plane normals parallel to the load axis was the plastically hard orientation. Intergranular strains developed linearly with plastic deformation to nearly 1% strain, saturating completely by 2.5% plastic strain.

Increasing temperature had a strong effect on both the strength of the material, and its ability to maintain intergranular and intragranular strains. The 0.2% offset yield point dropped from 315 MPa at room temperature, to 205 MPa at 200 °C, to 100 MPa at 400 °C. Similarly, the intergranular strains in the *b* direction, for instance, reduced from 2000 $\mu\varepsilon$ at room temperature, to 200 $\mu\varepsilon$ at 200 °C and are not significantly different from zero at 400 °C. Finally, the development of intragranular strains, measured by the diffraction peak breadth, is also significantly reduced with elevated deformation temperature. This behavior at temperature validates the traditional warm-rolling themo-mechanical processing of uranium plate.

When taken as a whole, this data is invaluable to future modeling efforts. The observed texture and internal strain development will act as constraint and validation for the development of predictive self-consistent plasticity models. The temperature dependent intergranular strains also provide input for model development, that is they imply a maximum residual stress at a given temperature.

Acknowledgements

This work has benefited from the use of the Lujan Neutron Scattering Center at LANSCE, which is funded by the Office of Basic Energy Sciences (DOE). Los Alamos National Laboratory is operated by Los Alamos National Security LLC under DOE Contract DE-AC52-06NA25396.

References

[1] J.W.L. Pang, T.M. Holden, P.A. Turner, et al., Acta Mater. 47 (1999) 373.
[2] M.A.M. Bourke, J.A. Goldstone, R.A. Robinson, Physica B 213/214 (1995) 806–808.
[3] M. Daymond, M. Bourke, R. Von Dreele, et al., J. Appl. Phys. 82 (1997) 1554.
[4] M.R. Daymond, M.A.M. Bourke, R.B. Von Dreele, J. Appl. Phys. 85 (1999) 739.
[5] M.R. Daymond, J. Appl. Phys. 96 (2004) 4263.
[6] R. Cahn, Acta Crystallogr. 4 (1951) 470.
[7] R.W. Cahn, Acta Metall. 1 (1953) 50.
[8] P.R. Morris (Ed.), ICOTOM-1, Krakow, Poland, 1971, p. 87.
[9] J. Daniel, B. Lesage, P. Lacombe, Acta Metall. 19 (1971) 163.
[10] C. Tomé, P. Maudlin, R. Lebensohn, et al., Acta Mater. 49 (2001) 3085.
[11] G. Kaschner, J. Bingert, C. Liu, et al., Acta Mater. 49 (2001) 3097.
[12] M. Bourke, D. Dunand, E. Ustundag, Appl. Phys. A 74 (2002) S1707.
[13] H. Wenk, L. Lutterotti, S. Vogel, Nucl. Instrum. Methods Phys. Res. A: Accel. Spectrom. Detectors Assoc. Equip. 515 (2003) 575.
[14] R.B. Von Dreele, J. Appl. Crystallogr. 30 (1997) 517.
[15] R.B. Von Dreele, J.D. Jorgensen, C.G. Windsor, J. Appl. Crystallogr. 15 (1982) 581.
[16] D. Brown, M. Bourke, B. Clausen, et al., Metall. Trans. A 34 (2003) 1439.
[17] S.R. MacEwen, J. Faber, A.P. Turner, Acta Metall. 31 (1983) 657.
[18] R.B. Fischer, J. Nucl. Mater. 18 (1966).
[19] P.A. Turner, C.N. Tome, Acta Metall. 42 (1994) 4143.
[20] T.M. Holden, unpublished results.
[21] A. Rollett (Ed.), Modeling the Deformation of Crystalline Solids, TMS, New Orleans, 1991, p. 361.
[22] D. Brown, R. Varma, M. Bourke, et al., ECRS 6, in: Proceedings of the 6th European Conference on Residual Stresses 404–4, 741, 2002.
[23] D.W. Brown, S.R. Agnew, M.A.M. Bourke, et al., Mater. Sci. Eng. A 399 (2005) 1.
[24] D.W. Brown, M.A.M. Bourke, P.S. Dunn, et al., Metall. Trans. A 32 (2001) 2219.
[25] R. Somasundaram, V. Premanand, J. Nucl. Mater. 19 (1966) 283.
[26] S.R. MacEwen, C. Tome, J. Faber, Acta Metall. 37 (1989) 979.
[27] C.N. Tomé, N. Turner, P. Miller, M. Woo, C.H. Root, J.T.M. Holden, J. Nucl. Mater. 227 (1996) 237–250.